



HAL
open science

Superior dielectric properties of epoxy-based photoresist thin film nanocomposites with carbon-coated Cu@C nanoparticles

C Lapeyronie, M Alfonso, B Viala, J-H Tortai

► To cite this version:

C Lapeyronie, M Alfonso, B Viala, J-H Tortai. Superior dielectric properties of epoxy-based photoresist thin film nanocomposites with carbon-coated Cu@C nanoparticles. *Materials Research Express*, 2022, 9 (10), pp.106301. 10.1088/2053-1591/ac9574 . hal-03807858

HAL Id: hal-03807858

<https://cnrs.hal.science/hal-03807858>

Submitted on 11 Oct 2022

HAL is a multi-disciplinary open access archive for the deposit and dissemination of scientific research documents, whether they are published or not. The documents may come from teaching and research institutions in France or abroad, or from public or private research centers.

L'archive ouverte pluridisciplinaire **HAL**, est destinée au dépôt et à la diffusion de documents scientifiques de niveau recherche, publiés ou non, émanant des établissements d'enseignement et de recherche français ou étrangers, des laboratoires publics ou privés.

Superior dielectric properties of epoxy-based photoresist thin film nanocomposites with carbon-coated Cu@C nanoparticles

C. LAPEYRONIE^{1*}, M.S. ALFONSO¹, B. VIALA², J.-H. TORTAI¹

¹ University Grenoble Alpes, CNRS, CEA/LETI-Minatec, Grenoble INP, Institute of Engineering and Management University Grenoble Alpes, LTM, Grenoble F-38054, France

² University Grenoble Alpes, CEA, LETI, 38000 Grenoble, France

*Corresponding author: (cedric.lapeyronie@cea.fr)

KEYWORDS: Metal Polymer Nanocomposites (MPCs), dielectric spectroscopy, nanoparticles, surface functionalization

ABSTRACT

The microelectronics community has shown great interest for high-k percolative nanodielectric materials for their applications as integrated capacitors. This work highlights the manufacturing process of high-quality Metal Polymer Nanocomposites (MPCs) thin dielectric films with Cu@C nanoparticles into SU8™ negative photolithographic resist. Four capacitor formulations from 0.8%vol up to 3.0%vol of Cu@C functionalized with an insulating layer of Polystyrene Pyrene-terminated (PyrPS) were produced. These films, with a targeted thickness of 15 μm, were spin-coated onto p-doped silicon wafers. Raman spectroscopy demonstrated the nature of the carbon shell of the nanoparticles and its effectiveness in protecting the core from oxidation, while SEM-EDS highlighted the uniformity of the nanoparticle distribution in the resist. Broadband dielectric spectroscopy measured an enhancement of ϵ_r to 124 with reasonable losses of 0.65 at 5 kHz for the (Cu@C)-PyrPS//SU8 3.0%vol nanocomposite. Through the use of Percolation Theory (PT) it was estimated the percolation threshold φ_c in the vicinity of 3.2%vol. Furthermore, no electrical aging or dielectric breakdown was detected at low voltage. All the results show the potential use of Cu@C nanoparticles to achieve a high-quality high-k MPC photoresists for the implementation as integrated capacitors.

INTRODUCTION

In recent decades, the microelectronics community has shown great interest in high dielectric constant nanocomposite (high-k) for the implementation of new nanocomposite materials for integrated capacitors^[1,2]. For instance, Metal Polymer Composites (MPCs) have received

considerable attention due to their wide versatility to address the different needs and constraints of such applications^[3,4]. In these materials the filling volume fraction, chemical composition, homogeneity of dispersions and shape of the nanoparticles (NPs) dictate the dielectric properties.

Previous studies stated that MPCs following Percolation Theory can exhibit high permittivity value at the vicinity of percolation threshold^[5,6]. However, the values of the reported dielectric losses are often irreconcilable to allow their practical applications^[7-10]. In fact, percolative nanodielectrics usually present a large increase in conductivity causing high dielectrics losses and making them not eligible as dielectric film capacitors^[9,10]. This latter undesirable effect is subordinate to the fact that nanoparticles tend to stay packed as aggregates and thus are complex to uniformly disperse in the polymeric matrix^[11,12]. Consequently, the achievement of a homogenous dispersion of NPs in a polymeric host is the crucial challenge to allow a fine tuning of these materials to combine high permittivity and low dielectric losses. For example, Lu *et al.*^[13] drew the conclusion that metallic silver (Ag) nanoparticles incorporated in carbon black/polymer composites enhance the dielectric constant of nanocomposite with value of 2260 at 10 kHz with dissipation factor of only 0.45 at 3.7%wt. Dang *et al.*^[14] have reported a percolative nanocomposite based on metallic nickel (Ni) nanoparticles randomly dispersed in PVDF showing a dielectric constant of 400 at 100 Hz and losses of 0.18 approaching percolation around 17%vol. Meeporn *et al.*^[15] claimed that ceramic nickelated Ag-MLSNO/PVDF nanocomposites can be used as a high-*k* material for energy storage applications with a dielectric constant of 62 at 1 kHz and low losses of 0.027 at a nanoparticle/polymer volume fraction of 17%vol. However, the reported values in literature vary over a wide range depending on the size of the nanoparticles, degree of nanostructuring and filling volume fraction percentage. Furthermore, most of the presented devices are millimetre thick and cannot be considered as suitable candidates for integrated capacitors.

Regarding all previous works, nanocomposites based on photolithographic resists seem to be the best suited materials to fit the needs of the microelectronics community in thin films with high dielectric constant. Following after this highly potential approach, this work aims to establish a wafer-scale film fabrication process using commercial carbon-coated copper nanoparticles (Cu@C), embedded in epoxy-based photoresist SU8™, to obtain a 15 μm thick capacitor with $\epsilon_r > 100$. The particles used were firstly chosen for their carbon shell, which will prevent the oxidation of the metallic core and thus, preserve the electrical properties of Cu. Secondly, the shell allow a non-covalent surface functionalization onto its graphene-like structure with a pyrene-terminated agent^[16,17]. The manufacturing process developed to obtain the

nanocomposite thin films is subdivided into five steps: NPs powder deagglomeration, surface functionalization, dispersion into the polymeric resist, spin-coating and photo-development of the formulated thin film nanocomposites, local gold electrode deposition. For the steps of deagglomeration, functionalization and dispersion, sono-mechanical treatments were performed^[18]. The dielectric properties of the formulated nanocomposite films were investigated by using broadband dielectric spectroscopy. Moreover, the effect of DC bias voltage on the dielectric properties was investigated. C–V loops highlighted a processable voltage window in which no evidence of electrical aging or dielectric breakdown was encountered. In the meantime, two mechanisms of electron field emission were observed as the filling volume fraction increases. The mentioned results were also modelled by using the percolation theory (PT) indicating a high dielectric constant of 124 in the vicinity of the percolation threshold (close to 3.2%vol).

Material and Methods

Chemicals

Nanopowders Cu@C with a nanoparticle mean diameter of 25 nm were purchased from Nanostructured & Amorphous Materials, Inc. Poly(styrene), Ω -(1-Pyrenyl)-Terminated (M_w/M_n 1.3) (PyrPS) supplied by Polymer Source was used as surface agent. Negative i-line epoxy photoresist SU8™2050, composed of epoxy resin, propylene carbonate, triaryl sulfonium initiator and cyclopentanone was supplied by Microresist Corp. Propylene glycol methyl ether acetate >99% (PGMEA) was purchased from Microposit™ EC Solvent.

Nanocomposites preparation

The aim of this manufacturing process is to produce film nanocomposites with a targeted thickness of 15 μm , in which nanoparticles are uniformly dispersed at different volume fractions (%vol). Thus, thin dielectric films are obtained through spin-coating deposition of formulated nanocomposites onto 4-inch Si Boron p-doped wafers (0.001-0.005 Ohm.cm) to make Metal-Insulator-Semiconductor (MIS) devices. Obtaining a homogeneous dispersion of nanopowders in high viscosity resist remains the main challenge of the nanofabrication process. Previous studies claimed that Van der Waals attraction and electrostatic repulsion are competing for the agglomeration of nanoparticles also during spin-coating deposition step. As a matter of fact, during the spin-coating step the NPs are driven into two directions enforced by two forces: (1) the centrifugation force that will align the particles radially and (2) the solvent evaporation force that will tend to stack particles vertically^[19]. The first force controls the thickness obtained via the

rotation speed of the spinner, while the second one depends on the casting solvent vapour pressure in regards with temperature and humidity. To limit the packing issue of the NPs, we developed a nanoformulation procedure involving ultrasonication of the nanoparticles in the PGMEA solvent, which entails a non-covalent surface functionalization prior to films deposition. The functionalisation step was performed by adding Polystyrene Pyrene-terminated (PyrPS) under bath sonication, in order to adsorb a thin insulating nanometric layer onto the Cu@C nanoparticles. This step was also used to improve the dispersibility of the nanoparticles in the SU8™ photoresist host as demonstrated by previous studies^[20,21].

Preliminary tests have given to the nanoparticles a concentration of 0.1 g/mL as the threshold limit to the achievement of a stable over time colloidal dispersion. Simultaneously, obtaining a targeted 15 µm thickness of the deposited nanocomposite films was achieved through coherent dilutions of the colloidal dispersion (Cu@C-PyrPS in PGMEA) and the photoresist. These dilutions allowed to maintain the same viscosity of the nanoformulations at different concentrations of nanoparticles. The complete fabrication of each nanocomposite consists in a five steps process as shown in Figure 1.

Step 1: Deagglomeration of Cu@C nanoparticles and surface functionalization with PyrPS in PGMEA in sonication bath Fisherbrand FB15055 at the power of 90 W. Nanoparticles and surface agent are added by small quantities, in alternation, to ensure good dispersion and functionalization. The totality of NPs powder is added in three times, as the PyrPS powder. Each addition of powder is followed by a 10 min sonication bath.

Step 2: Functionalized NPs are added into SU8™2050 photoresist and sono-mechanically dispersed by tip sonication for 30 minutes with QSONICA Sonicators Q500 at 100 W. In this step the SU8™2050 photoresist is diluted into a SU8™2010 photoresist.

Step 3: Spin-coating of 4 mL of nanocomposite resin onto a 4-inch wafer were performed by POLOS SPIN 200i at 1,500 rpm (with an acceleration of 5,000 rpm.s⁻¹) for 30 seconds to obtain a 15 µm thick film.

Step 4: Pre-bake, UV exposure and bake are performed on the spin-coated nanocomposite film. The two baking steps are performed with POLOS hotplate 200S (230 V_{AC}) at 95°C for 3 minutes and the UV exposure ($\lambda = 365$ nm) was done with a home-built mask aligner at a dose of 135 mJ/cm². Finally, the photodefinable nanocomposite is developed in PGMEA for 3 minutes.

Step 5: Deposition of 100 nm thick gold electrodes by using Physical Vapor Deposition (PVD) with PLASSYS Evaporation HV/UHV and a home-built mask for the implementation of MIS

devices. Film thickness was measured for each capacitor with a stylus profilometer (Bruker DektakXT).

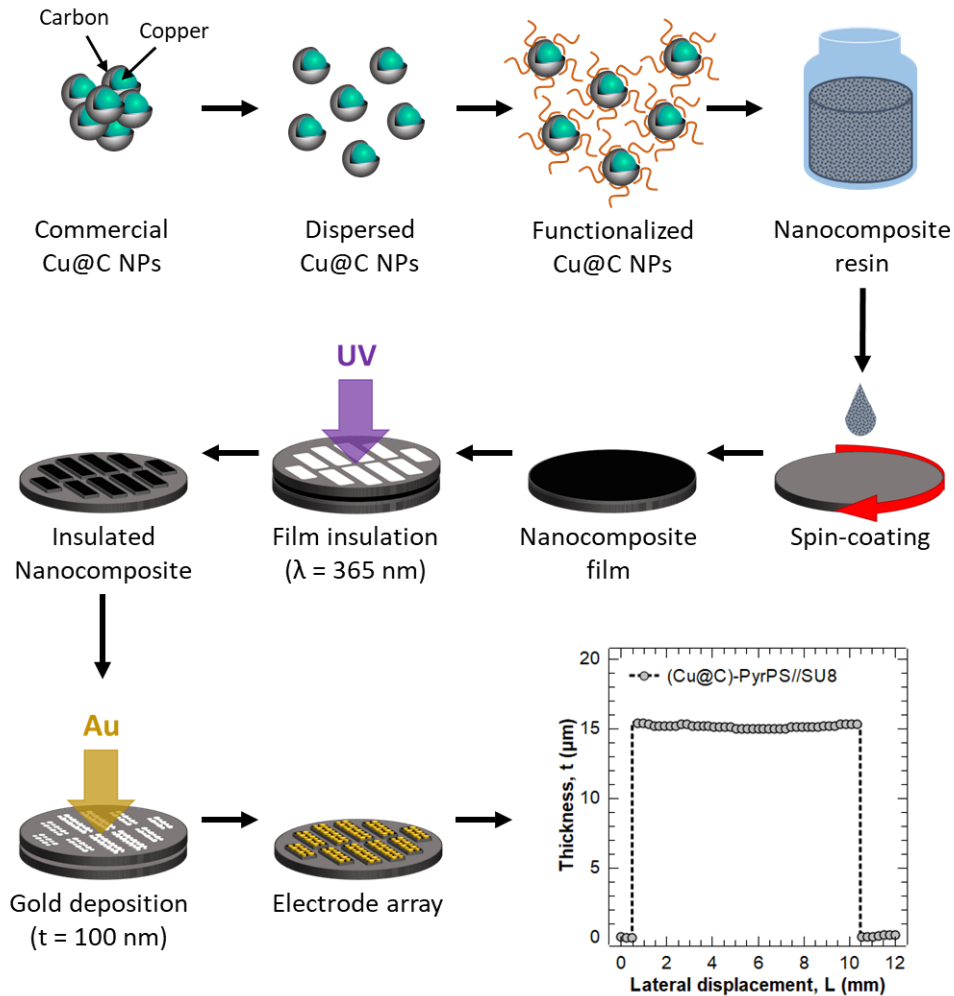


Figure 1 : Schematic of nanocomposite fabrication from commercial nanoparticles to the measurement of electrodes thickness.

Characterizations

To ensure the structure of the as received carbon-coated nanoparticles, Raman spectroscopy was performed on the raw powder. For this purpose, a beam of $\lambda=532 \text{ nm}$ was used to verify the absence of copper(II) oxide (CuO) and the nature of the carbonaceous shell coating the nanoparticles^[22]. Moreover, the morphology and chemical composition of the nanoformulated nanocomposite films were analysed by SEM/EDS cross sectional images and elemental mapping with ZEISS GeminiSEM. These characterisations allow to verify the dispersion

homogeneity of nanoparticles in the overall thickness of films and the effective chemical composition of the formulated films.

The dielectric behaviour of the nanoformulated nanocomposites thin films was investigated by using broadband dielectric spectroscopy (10^2 - 10^6 Hz) at room temperature using Novocontrol Alpha series ZG2 through a sinusoidal stimulation of $\pm 3V_{AC}$. The effects of DC voltage on the C-V and I-V characteristics were analysed by using Aixacct TF2000E at the frequency reference of 5 kHz. These measurements aimed to investigate the ageing, the occurrence of dielectric breakdown and the influence of NPs amount on the conduction mechanisms with an imposed DC bias voltage. Furthermore, to facilitate the comparison of these features, the obtained data were standardized over true electrodes thicknesses and surfaces.

RESULTS AND DISCUSSION

Nanocomposites structure

a) Raman spectroscopy

In order to verify the structure of the carbon shell and its integrity during the deagglomeration step, Raman spectroscopy was performed on sono-mechanically dispersed as-received Cu@C nanoparticles. The damaging of this protective shell during the manufacturing process could lead to the oxidation of the metallic copper core that can worsen the dielectric properties of nanocomposites. It can be noted that the thin carbon shell may be deteriorated also by the power of the beam used. For this reason, different laser powers were used to investigate the carbon structure. Firstly, the raw nanoparticles were excited with a beam power of 0.2 mW at a wavelength of 532 nm. The result shown in Figure 2.a presents the characteristic peaks of CuO which can be seen at 290 cm^{-1} , 340 cm^{-1} and 630 cm^{-1} ^[23]. Furthermore, the specific peaks for the graphene-like carbon^[24] located at 1587 cm^{-1} (G band) and 2700 cm^{-1} (2D band) are still visible, suggesting that the fragile carbon shell was partially destroyed due to the beam power. Thus, in order to avoid this damaging effect, the measurement was performed on another sample of the same composition at the same wavelength (532 nm) but at a lower laser power of 0.01 mW. In this case, Raman spectrum (Figure 2.b) does not reveal CuO peaks while the characteristic G band and 2D band are more intense. It can be concluded that the ultrasonicated as-received NPs exhibit no detectable oxidation and that the morphology of the carbon shell corresponds to a graphene-like structure. Despite the presence of a D band indicating the presence of defects inside the graphene crystalline structure, the carbon shell is efficient to protect the metal core

from oxidation. Moreover, the widen of the 2D band and the ratio of $I_{2D} / I_G \neq 2$ specify that we do not have a monolayer of graphene.

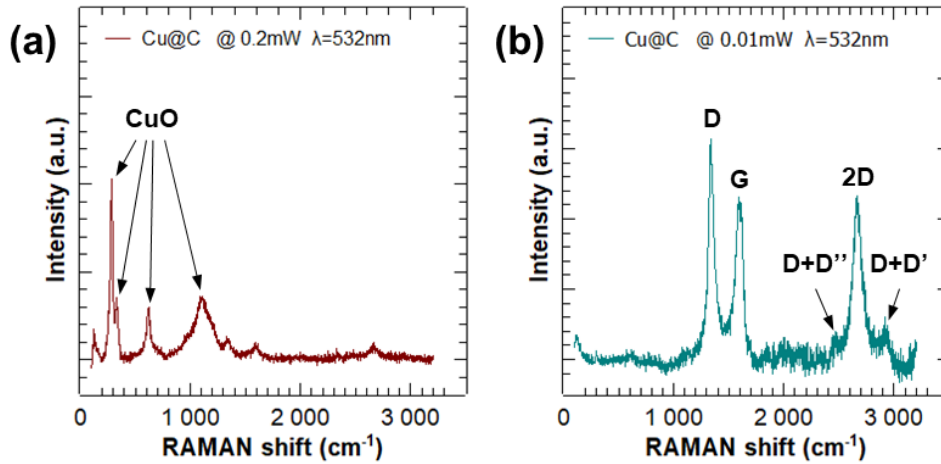


Figure 2 : Raman analysis of sono-mechanically dispersed as-received Cu@C nanoparticles at $\lambda = 532\text{nm}$ and at different powers. Raman spectrum at a beam power of (a) 0.2 mW and (b) at 0.01 mW.

b) Morphology of the nanocomposite films

To reach a manufacturing processing level, achieving a homogeneous dispersion of nanoparticles along the whole film thickness is essential. To ensure this goal, cross-sectional SEM micrograph coupled with EDS elemental mapping were performed on previously dielectric characterized MIS devices and are shown in Figure 3.

Figure 3.a presents a cross-sectional micrograph of the films, cut along the diameter of the circular electrodes. The images in Figure 3 show a low surface roughness with a highly nanostructured nanoparticles distribution, with different NPs size and shape in the overall film thickness. Moreover, a thickness of 15 μm film was measured, agreeing with the profilometry technique. This further elemental characterization confirms the efficiency of the sono-dispersion process on the homogenisation of the functionalised nanoparticles in the polymeric host (Figure 3 b and c).

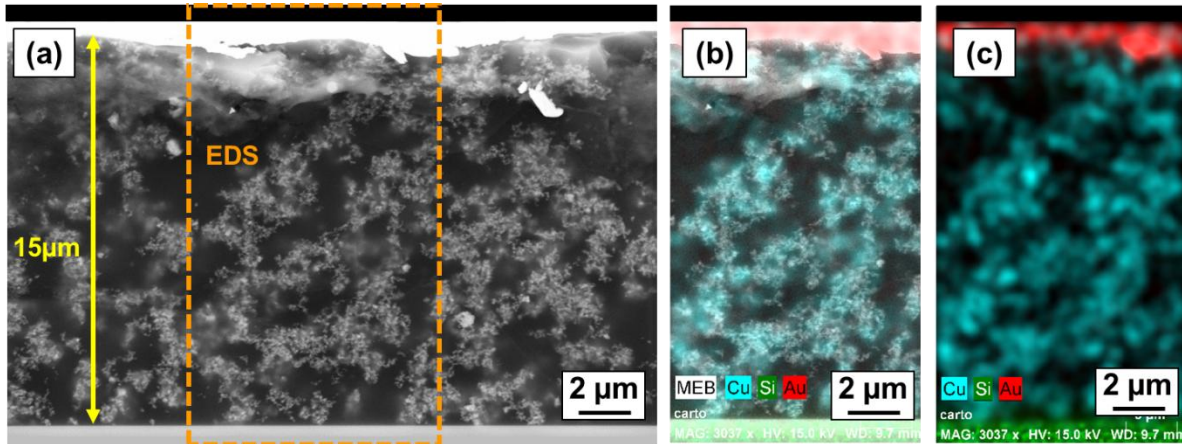


Figure 3: SEM micrograph coupled with EDS elemental mapping of (Cu@C)-PyrPS//SU8 2.4%vol. (a) Cross-sectional SEM micrograph of the targeted 15µm film thickness, (b) EDS elemental mapping superimposed to the SEM micrograph and (c) EDS elemental mapping.

Dielectric characterization

a) Dielectric spectroscopy

The dielectric behaviour of the (Cu@C)-PyrPS//SU8 (MIS) devices were characterized using a sinusoidal stimulation of $\pm 3 V_{AC}$ between 10^2 Hz and 10^6 Hz at room temperature. The frequency dependence of the characteristic dielectric features is shown in Figure 4.

The results have been averaged over 20 capacitors. Sampling on different locations of the deposited films on the same sample allowed to verify the distribution of Cu@C nanoparticles on it. No significant variation of the dielectric properties was detected confirming an equal distribution in the entire surface of the films. As frequently reported in literature, high-permittivity is often associated to high dielectric losses. Phase shift response was analysed to ensure the capacitive behaviour of formulated nanocomposites. Figure 4.a shows no significant variation of the phase angle with the volume fraction, up to 2.4%vol. In details, the phase angle remains close to -90° (pure capacitive behaviour) in the whole frequency range Hence, in this condition, the device can be modelled as a CPE (Constant Phase Element) at low volume fraction (lesser than 2.4%vol) and a RC parallel circuit exhibiting a typical frequency dependence of phase shift at higher volume fraction^[25]. Indeed, for the formulation at 3.0%vol of Cu@C the phase shift is close to -60° (mainly capacitive behaviour) at high frequencies ($f > 1$ kHz) then abruptly rises close to 0° (resistive behaviour) at low frequency. As shown in Figure 4.b, dielectric losses increase with volume fraction of Cu@C NPs. Nonetheless all the devices present losses inferior to the threshold value of 1 between 400 Hz and 10^6 Hz. However (Cu@C)-PyrPS//SU8 3.0%v shows an increase of $\tan \delta$ below 400 Hz with a maximum value of 4.30. This critical variation of

losses is in agreement with the previously discussed phase shift frequency dependence. It can be attributed to the low inversion of electric field applied that facilitates charges mobility, thus, preventing the storage of charges.

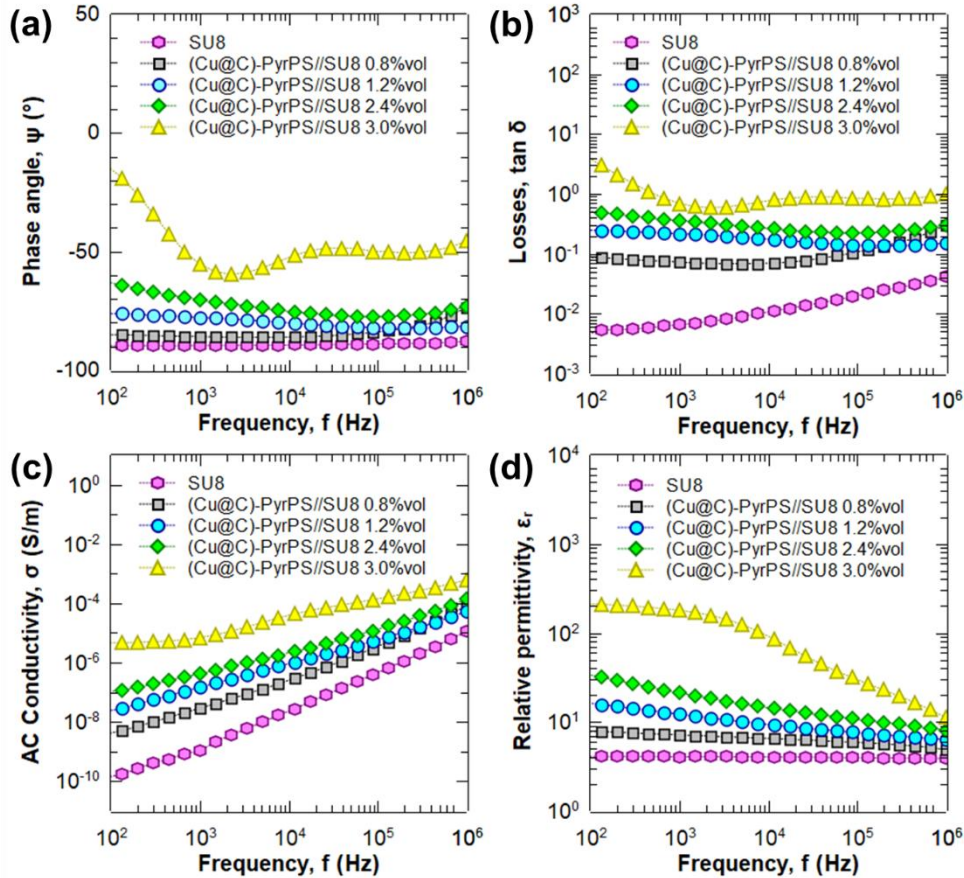


Figure 4: Frequency dependence of the (a) phase angle Ψ , (b) dielectric losses expressed as $\tan\delta$, (c) AC conductivity σ and (d) relative permittivity ϵ_r of (Cu@C)-PyrPS/SU8 nanocomposites with different filling volume fraction.

The frequency dependence of AC conductivity is shown in Figure 4.c. A linear response of AC conductivity was measured for all formulated nanocomposites except for the highest loaded composite which exhibits a constant value of AC conductivity at low frequency, typical of a resistive behaviour. Finally, it is shown in Figure 4.d an increment of the relative permittivity of the formulated nanocomposites as the volume fraction increases. The highest permittivity obtained at the reference frequency value of 5 kHz was measured for the sample at the highest concentration, with a permittivity value of 124. This value is one order of magnitude higher of

pure SU8™ polymer. In Table 1 below are reported the values of the previously discussed dielectric parameters at the reference frequency of 5 kHz.

Table 1: Dielectric properties of the (Cu@C)-PyrPS//SU8 nanocomposites measured at 5 kHz and $\pm 3 V_{AC}$

	Ψ (°)	σ (S/m)	$\tan \delta$	ϵ_r
SU8	-89.539	1.026×10^{-8}	0.0089	4.053
0.8%v	-86.091	1.309×10^{-7}	0.0683	6.697
1.2%v	-79.266	5.444×10^{-7}	0.1896	10.046
2.4%v	-73.880	1.319×10^{-6}	0.2891	15.920
3.0%v	-56.762	2.294×10^{-5}	0.6561	123.669

This variation of permittivity could be explained by the Maxwell-Wagner-Sillars theory (MWS)^[26,27]. The MWS theory also known as interfacial polarization takes place when two phases present an ϵ_r and σ different. Under the influence of an external electric field, electrical charges accumulate at the interface between the matrix and the fillers. In this study, the charges accumulate at the interface between the SU8™ and the functionalized (Cu@C)-PyrPS. Consequently, increasing the filling volume fraction of nanoparticles rise the quantity of charges inside the material leading to an enhancement of capacitance, and thus relative permittivity. However, this is only true before electrical percolation. Once electrical percolation is reached current can flow through the material and the capacitance drops while the losses rise drastically. The results are also supported by the percolation theory stating that permittivity and losses follow a power law with an exponential increase at the vicinity of the percolation threshold^[6]. Indeed, as the number of nanoparticles in the matrix increases, the interparticular distance lowers easing conduction mechanisms. Considering the values presented in Table 1 the variation of all four dielectric parameters suggests that none of the presented nanocomposites reached the percolation threshold. The large variation of permittivity between 2.4%vol and 3.0%vol on the contrary seems to indicate percolation threshold is not reached yet.

By Comparing the obtained experimental results with the literature, the capacitive nanocomposites produced does not exhibit giant permittivity in the proximity of percolation threshold. However, at the reference frequency of 5 kHz the dielectric losses $\tan \delta$ is 0.65. This obtained value for the highest capacitive nanocomposite (3.0%vol) is not so low but still usable in practical applications. As a comparison, Wang *et al.*^[9] presented PDMS filled with carbon nanotube with ϵ_r of 60 and $\tan \delta$ of 10 (@ 10 kHz) for MWCNTs/PDMS 2%wt and Cao *et al.*^[8]

showed a SiC-PVDF 20%wt nanocomposite with ϵ_r of 200 and $\tan \delta$ of 8 (@ 5 kHz). In consequence, our most charged formulation presents a direct improvement of nanocomposite thin film, as capacitor, with high permittivity and low losses.

b) Percolation Theory and percolation threshold estimation

The value of percolation threshold was estimated by using the generalized power laws of percolation as shown below in equation 1 and 2. Equation 1 details the variation before percolation threshold while equation 2 details the variation after percolation threshold:

$$\epsilon_{eff} = \epsilon_m \left(\frac{\varphi_c - \varphi}{\varphi_c} \right)^{-s} \quad \sigma_{eff} = \sigma_m \left(\frac{\varphi_c - \varphi}{\varphi_c} \right)^{-t} \quad \varphi < \varphi_c \quad (\text{eq. 1})$$

$$\epsilon_{eff} = \frac{1}{\epsilon_m (\varphi - \varphi_c)^s} \quad \sigma_{eff} = \sigma_{NP} \left(\frac{\varphi - \varphi_c}{1 - \varphi_c} \right)^t \quad \varphi > \varphi_c \quad (\text{eq. 2})$$

Where ϵ_{eff} is the effective relative permittivity, ϵ_m is the relative permittivity of the polymeric matrix, σ_{eff} is the effective conductivity, σ_m is the conductivity of the matrix, σ_{NP} is the conductivity of a nanoparticle, s and t are the critical exponents for permittivity and conductivity respectively. In Figure 5 is shown the obtained values at 5 kHz of AC conductivity and relative permittivity with the fit obtained with the percolation theory power laws.

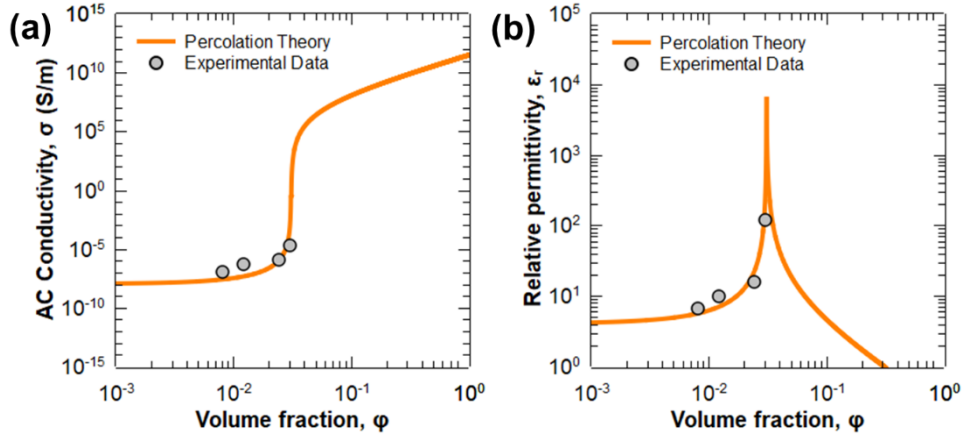


Figure 5 : Percolation theory applied to the experimental values. Fit of experimental data at 5 kHz and 3 V_{AC} on: (a) Conductivity, (b) Relative permittivity

This model fits quite precisely the experimental obtained data and estimates the percolation threshold at the proximity of $\varphi_c \approx 3.2\%vol$ with $s = 1.1$ and $t = 3$. The critical exponents are in agreement with what is reported in literature although these values slightly vary according to the specific conductivity of nanostructured system^[28-30]. In agreement with the estimation of percolation threshold the highest loaded sample of 3.0%vol displays all the dielectric features of a classic behaviour of a near percolated system. That is why samples at higher volume fraction were not investigated in this study.

c) Effect of Bias DC voltage on dielectric properties

The dielectric responses of the formulated Cu@C based nanocomposites in response to an applied DC electric field obtained with AIXACCT TF2000E are reported on Figure 6. In details, the maximum value of sustained DC electric field is represented for each nanocomposite. It is worthy to note that above these reported values, the conduction mechanisms of charges transport increase significantly turning the devices into highly leaky capacitors. As a matter of fact, above these values it is prevented to make measurements with this technique due to the abrupt increase of dissipative current.

The obtained relative permittivity values obtained through C-V loop measurements are in accordance with the previously characterized ones obtained by dielectric spectroscopy (@ 5 kHz) as shown in Figure 6.a. No variations of permittivity are visible on the range of electric field applied. DC voltage do not seem to have an impact on the polarisation of the material. However, the sustained DC voltage is dependent of the filling volume fraction. Particularly, the high loaded nanocomposite (Cu@C)-PyrPS//SU8 3.0%vol can stand an electric field of ± 6.01 kV/cm while the (Cu@C)-PyrPS//SU8 0.8%vol can withstand an electric field of ± 33.88 kV/cm.

The effects of a DC bias electric field are highlighted in the evolution of dielectric losses as shown in Figure 6.b. Indeed, for the formulation at 3.0%vol the dielectric losses response assumes a flat trend with a value of 0.68, in accordance to dielectric spectroscopy, at low applied DC electric field up to the threshold value of 3.51 kV/cm where the dielectric losses suddenly increase leading to a leaky capacitor. This effect is present in all formulated nanocomposites with the DC electric field threshold value decreasing with the increase of volume filling fraction.

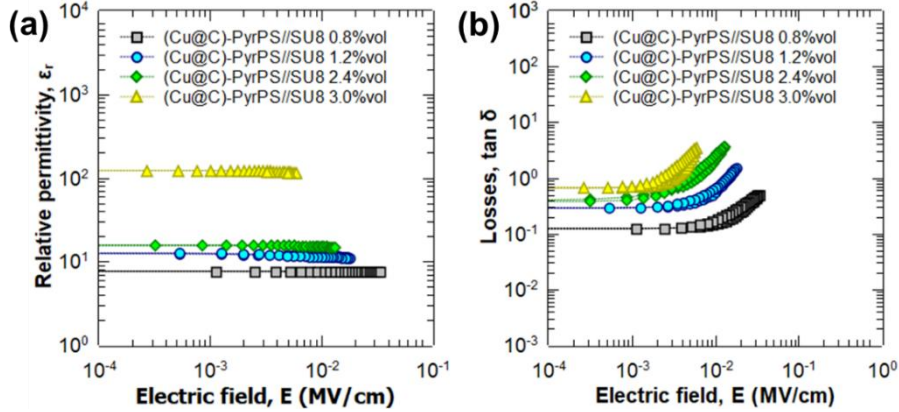


Figure 6: (a) Relative permittivity and (b) losses as $\tan\delta$ as function of DC electric field at 5 kHz for formulated (Cu@C)-PyrPS//SU8 nanocomposite thin films

In order to evaluate the conduction mechanisms involved in this dramatically increase of dielectric losses under the application of an DC electric field, the charge transport regimes were investigated. Figure 7.a. shows the non-linear dependence of current density under DC applied electric field, following the same trend as dielectric losses.

A greater level of understanding can be achieved through the representation of logarithm of current density over electric field as a function of the inverse of applied electric field^[31,32]. This representation (Figure 7.b) allows to distinguish a minimum value that correspond to a transition between two different conduction mechanisms. These phenomena are the Direct Tunnelling and Fowler-Nordheim Tunnelling conduction.

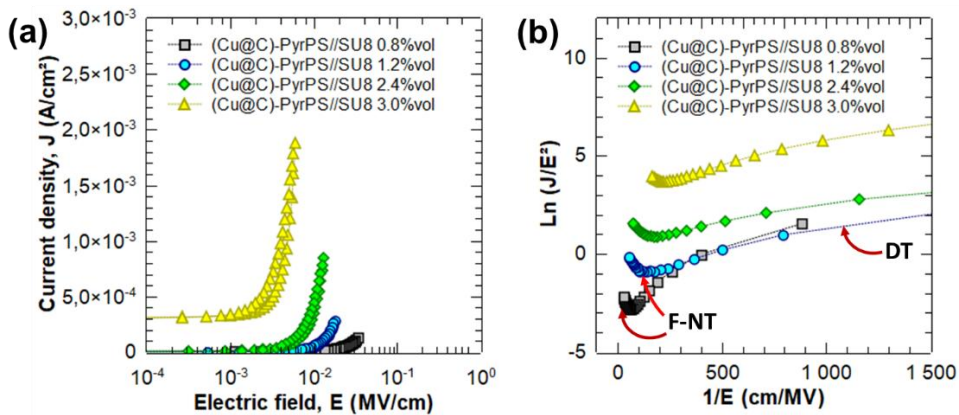


Figure 7: (a) Current density as function of DC electric field, (b) Logarithm of current density over DC electric field as a function of the inverse of DC electric field at 5 kHz for formulated (Cu@C)-PyrPS//SU8 nanocomposite thin films

The conduction mechanisms which takes place in the material are dependant of the nanostructured system. In details, the mobility of charges that flow through the nanofillers is function of the distance between them and thus depending on their distribution and quantity. Indeed, at low applied DC electric field the energy given to the charges is enough to go through small energy barrier. As a result, the displacement of charges will only be on close fillers (Direct Tunnelling).

However, above the threshold E_{Trans} determined by the inflection of the curves as shown in Figure 7.b, charges which are intrinsic of the metallic nanofillers are emitted on long distances (Fowler-Nordheim Tunnelling) brutally increasing the current density of the nanocomposites. Thus, with the increase of volume filling fraction the energy barrier length through the nanofillers decrease with the occurrence of the Fowler-Nordheim tunnelling at lower applied DC electric field. The obtained E_{Trans} values determined for each nanocomposite is summarized in Table 2.

Table 2: Values of transition electric field between Direct tunnelling and Fowler-Nordheim tunnelling for all formulated nanocomposites

@ 5 kHz	0.8%v	1.2%v	2.4%v	3.0%v
$1/E_{\text{Trans}}$ (cm/MV)	62.008	128.016	174.910	221.888
E_{Trans} (MV/cm)	1.613×10^{-2}	7.812×10^{-3}	5.717×10^{-3}	4.507×10^{-3}

CONCLUSION

This article presents a reliable fabrication path for the achievement of homogeneous Metal Polymer Composites (MPCs) thin films based on Cu@C nanoparticles embedded in SU8™ photoresist with a controlled thickness of 15 μm. Raman spectroscopy performed on the as-received Cu@C nanoparticles showed the graphene-like structure necessary for the surface functionalization by Polystyrene Pyrene terminated (PyrPS). The dielectric properties determined by broadband dielectric spectroscopy showed an ϵ_r 31 times higher than pure SU8™ with reasonable losses $\tan \delta$ of 0.65 at 5 kHz for the highest filled formulation (3.0%vol). The Percolation Theory used on the dielectrical parameters allowed to establish the percolation threshold φ_c of the system to be at the vicinity of 3.2%vol. Superior capacitive behaviour was observed for the (Cu@C)-PyrPS//SU8 3.0%vol up to an applied DC electric field of 3.51 kV/cm and no breakdown appeared until 6.01 kV/cm. Finally, it was observed two conduction mechanisms depending on the intensity of the electric field: Direct tunneling and Fowler-Nordheim tunneling.

ACKNOWLEDGEMENT

This work was funded by the French IPCEI NANO 2022 Murata program and was partly supported by PTA (Upstream Technological Platform), cooperated by CNRS RENATECH and CEA Grenoble, France. The Raman spectroscopy was performed by LE Van-Hoan (DRT/LETI/DPFT/SMCP/LPMS) CEA Grenoble, France.

REFERENCES

- [1] Shimoga G and Kim S-Y 2020 High-k Polymer Nanocomposite Materials for Technological Applications *Applied Sciences* **10** 4249
- [2] Toor A, So H and Pisano A P 2017 Dielectric properties of ligand-modified gold nanoparticle/SU-8 photopolymer based nanocomposites *Applied Surface Science* **414** 373–9
- [3] Xu J and Wong C P 2007 High dielectric constant SU8 composite photoresist for embedded capacitors *J. Appl. Polym. Sci.* **103** 1523–8
- [4] Mendes-Felipe C, Barbosa J C, Gonçalves S, Pereira N, Costa C M, Vilas-Vilela J L and Lanceros-Mendez S 2020 High dielectric constant UV curable polyurethane acrylate/indium tin oxide composites for capacitive sensing *Composites Science and Technology* **199** 108363
- [5] Stauffer D and Aharony A 2018 *Introduction to percolation theory* (Taylor & francis)
- [6] Yuan J 2017 Percolation of carbon nanomaterials for high-k polymer nanocomposites *Chinese Chemical Letters* **28** 2036–44
- [7] Liao S, Shen Z, Pan H, Zhang X, Shen Y, Lin Y-H and Nan C-W 2017 A surface-modified TiO₂ nanorod array/P(VDF–HFP) dielectric capacitor with ultra high energy density and efficiency *J. Mater. Chem. C* **5** 12777–84
- [8] Cao X, Zhao W, Gong X, Zhang D, Su Q, Zha J, Yin X, Wu W and Li R K Y 2021 Mussel-inspired polydopamine functionalized silicon carbide whisker for PVDF composites with enhanced dielectric performance *Composites Part A: Applied Science and Manufacturing* **148** 106486
- [9] Wang Z, Li X, Wang L, Li Y, Qin J, Xie P, Qu Y, Sun K and Fan R 2020 Flexible multi-walled carbon nanotubes/polydimethylsiloxane membranous composites toward high-permittivity performance *Adv Compos Hybrid Mater* **3** 1–7

- [10] Li Y-J, Xu M, Feng J-Q and Dang Z-M 2006 Dielectric behavior of a metal-polymer composite with low percolation threshold *Appl. Phys. Lett.* **89** 072902
- [11] Liu J, Gao Y, Cao D, Zhang L and Guo Z 2011 Nanoparticle Dispersion and Aggregation in Polymer Nanocomposites: Insights from Molecular Dynamics Simulation *Langmuir* **27** 7926–33
- [12] Rishi K, Narayanan V, Beaucage G, McGlasson A, Kuppa V, Ilavsky J and Rackaitis M 2019 A thermal model to describe kinetic dispersion in rubber nanocomposites: The effect of mixing time on dispersion *Polymer* **175** 272–82
- [13] Lu J, Moon K-S, Xu J and Wong C P 2006 Synthesis and dielectric properties of novel high-K polymer composites containing in-situ formed silver nanoparticles for embedded capacitor applications *J. Mater. Chem.* **16** 1543
- [14] Dang Z-M, Lin Y-H and Nan C-W 2003 Novel Ferroelectric Polymer Composites with High Dielectric Constants *Adv. Mater.* **15** 1625–9
- [15] Meeporn K and Thongbai P 2019 Improved dielectric properties of poly(vinylidene fluoride) polymer nanocomposites filled with Ag nanoparticles and nickelate ceramic particles *Applied Surface Science* **481** 1160–6
- [16] Alfonso M S, Viala B and Tortai J-H 2019 Core-Shell Percolative Nanodielectric for High Voltage Integrated Capacitors *Journées nationales sur les technologies émergentes en micro-nano fabrication, (JNTE2019)*
- [17] Takacs H, Viala B, Herman V, Alarcon Ramos J, Tortai J-H and Duclairoir F 2015 New Approach to Closely Spaced Disordered Cobalt–Graphene Polymer Nanocomposites for Non-Conductive RF Ferromagnetic Films *IEEE Trans. Magn.* **51** 1–4
- [18] Dieringa H 2018 Processing of Magnesium-Based Metal Matrix Nanocomposites by Ultrasound-Assisted Particle Dispersion: A Review *Metals* **8** 431
- [19] Ogi T, Modesto-Lopez L B, Iskandar F and Okuyama K 2007 Fabrication of a large area monolayer of silica particles on a sapphire substrate by a spin coating method *Colloids and Surfaces A: Physicochemical and Engineering Aspects* **297** 71–8
- [20] Alfonso M S, Lapeyronie C, Goubet M, Viala B and Tortai J H 2021 Enhanced dielectric properties of epoxy-based photoresist nanocomposites using carbon-coated nickel nanoparticles for high voltage integrated capacitors *Composites Science and Technology* **216** 109063
- [21] Takacs H, Viala B, Tortai J-H, Hermán V and Duclairoir F 2016 Non-conductive ferromagnetic carbon-coated (Co, Ni) metal/polystyrene nanocomposites films *Journal of Applied Physics* **119** 093907

- [22] Ebnesajjad S 2011 Surface and Material Characterization Techniques *Handbook of Adhesives and Surface Preparation* (Elsevier) pp 31–48
- [23] Xu J F, Ji W, Shen Z X, Li W S, Tang S H, Ye X R, Jia D Z and Xin X Q 1999 Raman spectra of CuO nanocrystals *J. Raman Spectrosc.* **30** 413–5
- [24] Robertson J 2002 Diamond-like amorphous carbon *Materials Science and Engineering R* **37** 129–251
- [25] Gompf B, Dressel M and Berrier A 2018 Impedance spectroscopy and equivalent circuits of metal-dielectric composites around the percolation threshold *Appl. Phys. Lett.* **113** 243104
- [26] Van Beek L K H 1960 The Maxwell-Wagner-Sillars effect, describing apparent dielectric loss in inhomogeneous media *Physica* **26** 66–8
- [27] Perrier G and Bergeret A 1997 Polystyrene-glass bead composites: Maxwell-Wagner-sillars relaxations and percolation *J. Polym. Sci. B Polym. Phys.* **35** 1349–59
- [28] Yacubowicz J and Narkis M 1986 Dielectric behavior of carbon black filled polymer composites *Polym. Eng. Sci.* **26** 1568–73
- [29] Nan C-W 1993 PHYSICS OF INHOMOGENEOUS INORGANIC MATERIALS *PROGRESS IN MATERIALS SCIENCE* **37** 1–116
- [30] Clarkson M T 1988 Electrical conductivity and permittivity measurements near the percolation transition in a microemulsion. II. Interpretation *Phys. Rev. A* **37** 2079–90
- [31] Zhang G, Li Y, Tang S, Thompson R D and Zhu L 2017 The Role of Field Electron Emission in Polypropylene/Aluminum Nanodielectrics Under High Electric Fields *ACS Appl. Mater. Interfaces* **9** 10106–19
- [32] Ikuno T, Okamoto H, Sugiyama Y, Nakano H, Yamada F and Kamiya I 2011 Electron transport properties of Si nanosheets: Transition from direct tunneling to Fowler-Nordheim tunneling *Appl. Phys. Lett.* **99** 023107